Journal of Magnetic Resonance 339 (2022) 107217

Contents lists available at ScienceDirect

Journal of Magnetic Resonance

journal homepage: www.elsevier.com/locate/jmr

How accurately defined are the overtone coefficients in Gd(III)-Gd(III) RIDME?

Mykhailo Azarkh [a,*], Katharina Keller [b], Mian Qi [c], Adelheid Godt [c], Maxim Yulikov [b,*]

[a] Department of Chemistry, University of Konstanz, Universitätsstraße 10, 78457 Konstanz, Germany
[b] Laboratory of Physical Chemistry, Department of Chemistry and Applied Biosciences, ETH Zurich, Vladimir-Prelog-Weg 2, 8093 Zurich, Switzerland
[c] Faculty of Chemistry and Center for Molecular Materials (CM2), Bielefeld University, Universitätsstraße 25, 33615 Bielefeld, Germany

ARTICLE INFO

Article history:
Received 1 February 2022
Revised 4 April 2022
Accepted 5 April 2022
Available online 9 April 2022

Keywords:
Gd(III)
Py-MTA
Molecular ruler
Overtone coefficients
RIDME
EPR

ABSTRACT

Relaxation-induced dipolar modulation enhancement (RIDME) is a pulse EPR technique that is particularly suitable to determine distances between paramagnetic centers with a broad EPR spectrum, e.g. metal-ion-based ones. As far as high-spin systems (S > ½) are concerned, the RIDME experiment provides not only the basic dipolar frequency but also its overtones, which complicates the determination of inter-spin distances. Here, we present and discuss in a step-by-step fashion an r.m.s.d.-based approach for the calibration of the overtone coefficients for a series of molecular rulers doubly labeled with Gd(III)-PyMTA tags. The constructed 2D total-penalty diagrams help revealing that there is no unique set of overtone coefficients but rather a certain pool, which can be used to extract distance distributions between high-spin paramagnetic centers, as determined from the RIDME experiment. This is of particular importance for comparing RIDME overtone calibration and distance distributions obtained in different labs.

1. Introduction

Pulse dipolar spectroscopy (PDS) in EPR offers a powerful set of techniques to determine distances between unpaired electrons [1,2]. When combined with site-directed spin labelling [3–5], PDS becomes a valuable tool in structural biology, allowing to determine structure of biomacromolecules [6,7] or biomolecular complexes [8] and to follow structural changes they undergo [9]. Depending on the number of subunits in a biomolecule or biomolecular complex under study, as well as on the sample preparation conditions, a certain type of spin label or a combination of different types of spin labels can be used [10–12]. Besides the nitroxide-based spin labels, substantial attention has been paid in the last few years to optimize PDS approaches for paramagnetic metal-ion-based spin labels [13–18]. In particular, Gd(III)-based spin labels attract significant attention, since they exhibit favorable relaxation properties and stability against intracellular reduction [19–23]. Relaxation-induced dipolar modulation enhancement (RIDME) is one of the possible PDS experiments for distance determination with spin pairs that include Gd(III) ions [24–26]. Given the fact that a spectrum of Gd(III) spreads over up to 2 GHz, a particular advantage of RIDME is that for all excited observer spins, the coupling to partner spins is detected regardless of the resonance frequency of the latter, without requiring large resonator bandwidth or excitation bandwidth of the microwave pulses.

Here, we take an example of the Gd(III)-Gd(III) RIDME experiment, for which the largest set of experimental data and analysis was published up to date [27–30]. Since, in the Gd(III)-Gd(III) RIDME experiment, the modulation due to the dipolar spin-spin coupling is induced by spontaneous spin flips, dipolar frequency overtones (DFOs) are excited in addition to the main dipolar frequency. Their relative contributions are determined by the probabilities of changing the electron spin projection by more than one quantum either in a single spin flip or after multiple spin flips. The presence of such overtones complicates data processing. If not accounted properly during the data processing, DFOs lead to artifacts in the distance distribution. Consequently, for distance determination by Gd(III)-Gd(III) RIDME, the fractions of DFOs have to be taken into account. So far the most detailed calibration of DFO coefficients (DFOCs) was performed on a series of Gd-PyMTA-based spectroscopic rulers [27,30] and revealed several important points:

(i) Only the primary dipolar frequency and its double and triple harmonics need to be taken into account, while the contributions from higher harmonics are negligible;

* Corresponding authors.
E-mail addresses: mykhailo.azarkh@uni-konstanz.de (M. Azarkh), maxim.yulikov@phys.chem.ethz.ch (M. Yulikov).

https://doi.org/10.1016/j.jmr.2022.107217
1090-7807/

(ii) DFOCs appear nearly perfectly constant within the RIDME mixing time, and almost constant within the practically relevant temperature range;
(iii) DFOCs are distance-dependent for inter-spin distances below 3.0 nm, while they become approximately distance-independent for distances above 3.0 nm;
(iv) The RIDME data fitting is rather sensitive to the proper selection of the ratio between the weight of the primary dipolar frequency and the sum of the weights of the second and third DFO, while the quality of the data fit is only weakly dependent on the small variations of the two DFOCs as long as their sum is kept constant;
(v) For the quality of the DFO calibration, it is important to use reference samples with narrow distance distributions, so that artifact distance peaks due to DFOs are resolved. Please note that these findings are specifically for the Gd-PyMTA-based rulers, and should be transferred to other Gd(III) complexes with care.

The negligibly weak contributions from higher overtones point to a transient balance rather than an established thermodynamic equilibrium of the spin states of the partner spins. The complete physical picture behind this balance of DFOs might not yet be established in full detail. This, however, does not prevent establishing the fact that such a balance is present for Gd(III) biradicals. This is accounted for by the calibration of DFOCs on a series of reference samples with narrow distance distributions. For distances above the threshold of 3.0 nm, where DFOCs become distance independent, a single set of DFOCs can be established. Essentially, this procedure consists of determining the best set of DFOCs for each reference sample and then establishing an "average set" of DFOCs that would result in the minimal error over the calibration set. While the last step is methodologically clear and depends in an unambiguous way on the type of the penalty function taken for the error determination, the step of determining this penalty function and the best set of DFOCs for each reference sample potentially allows for different solutions. Consequently, the resulting set of DFOCs is not necessarily a unique one.

Slightly different sets of DFOCs appear as a result of different background corrections, variation in noise level and the presence of distance distribution artifacts that are not due to the DFOs. For instance, it has been proposed recently that the DFOCs for Gd-PyMTA-based rulers are slightly different in D_2O and H_2O [30]. While this difference might in principle point to the change of the DFOCs upon the change of the spin label environment (protonated vs. deuterated glassy solvent), the differences in the fit quality between the two mentioned sets of the DFOCs are not particularly large, which implies that the differences in the values of the DFOCs might also be a result of differences in the calibration procedures. Since we expect that the topic of calibrating DFOCs for different types of Gd(III) complexes will be of importance in the near future, we consider it important to re-discuss the calibration procedure of the DFOCs in detail and, most importantly, determine the accuracy limitations of this procedure.

Here, we present a detailed step-by-step discussion of a DFOCs calibration procedure for Gd(III)-Gd(III) RIDME experiment performed for a series of Gd-PyMTA-based rulers. This allows us to compute 2D total-penalty diagrams nicely visualizing the area within which DFOCs can be potentially selected. In order to present a general approach for different paramagnetic center combinations, and also in view of occasional differences between DEER and RIDME data due to orientation selection, or due to the known Gd(III)-Gd(III) DEER distortions at short spin-spin distances, [31] we performed here a DFOCs calibration that does not use any auxiliary DEER data. The paper is organized as follows. First, we discuss the key steps in determining the best set of DFOCs for one particular sample. This includes the analysis of the background correction procedure, the form factor fit quality, and the artifact distance peaks intensities. Second, we discuss the determined range of possible solutions. Finally, we summarize the output of the analogous detailed analysis for other Gd-PyMTA-based rulers and give a comparison of the DFOCs calibration of one Gd-PyMTA-based ruler in protonated and deuterated matrix.

2. Experimental details and data analysis procedures

2.1. Gd-PyMTA-based rulers

Stiff molecular rulers that bear two Gd-PyMTA complexes connected by a linear shape-persistent linker were used [27,32,33]. The distances between the Gd(III) ions in these rulers were 2.1, 3.0, 3.4, 4.3, 4.7, and 6.0 nm [27,30]. RIDME samples were prepared by dissolving the rulers in either D_2O or H_2O (20–50% by volume glycerol-d_6 or glycerol, respectively) to yield a final ruler concentration in the range of 25–300 μM [27,30].

2.2. RIDME measurements

RIDME measurements were performed at Q- and/or W-band, as reported recently. The details are given elsewhere [27,30]. For each interspin distance one set of data was selected. The corresponding temperature and mixing times are given in Table 1.

2.3. Data analysis

Data analysis was performed with Matlab. Built-in functions from OvertoneAnalysis were used for processing of the experimental data, background correction, and Tikhonov regularization.

2.3.1. Background correction

A background model was chosen by selecting the background start of the RIDME time trace and fitting a stretched exponential to it. The penalty functions for the background corrections were defined as r.m.s.d. values for the fits of the form factor and the Pake pattern, which were obtained after processing the background corrected data with Tikhonov regularization disregarding DFOs, i.e. $\{P_1 = 1, P_2 = P_3 = 0\}$.

2.3.2. Fit quality as a function of DFOCs

The form factor obtained after the background correction was processed by Tikhonov regularization, while the kernel function contained a pre-defined set of DFOCs $\{P_1, P_2, P_3\}$. The two penalty functions related to this set of DFOCs were the r.m.s.d. values for the fits of the form factor and the Pake pattern.

2.3.3. Artifacts in the distance distribution

DFOCs, when under- or overestimated, produce artifacts in the distance distribution below or above the expected distance, respectively. The penalty functions with respect to these distance artifacts were computed as follows. A distance distribution obtained by Tikhonov regularization as described above was normalized to the intensity at the expected distance (i.e. at 2.1, 3.0, 3.4, 4.3, 4.7, and 6.0 nm, according to the molecular rulers used) and cut at this distance into two parts. For each sub-distribution, the distance probabilities were summed up separately; each of the two resulting numerical values contained the contributions from the artifact distances and a constant contribution from the real distances. From this procedure, two distance penalty functions for a given set of DFOCs were obtained: the first one for the distance artifacts below the expected distance, in the following lower-distance penalty function, and the second one for the

Table 1
Selected experimental parameters for the datasets used.

	2.1 nm	3.0 nm (prot.)	3.0 nm (deut.)	3.4 nm	4.3 nm	4.7 nm	6.0 nm
Mixing time, μs	12	8	12	10	24	24	16
Temperature, K	20	10	10	20	10	10	10
MW band	W	Q	W	W	W	W	W

distance artifacts above the expected distance, in the following upper-distance penalty function.

2.3.4. Error bars for DFOCs

The error bars were calculated from the total-penalty diagram. First, the minimum total penalty was found. Second, an area on the total-penalty diagram was determined, which corresponds to 10% deviation from the minimum total penalty. The DFOCs were read out from this area. For each DFOC, a minimum and maximum value was read out and assigned to the lower and upper limit for the error bar, respectively.

3. Results and discussion

3.1. General approach to calibrate DFOCs

The calibration of DFOCs is performed for a series of experimental RIDME data collected for molecular rulers with a narrow distance distribution. For each molecular ruler, a background corrected form factor is processed for all combinations of DFOCs, which are systematically varied, and for each combination of DFOCs the distance distribution is obtained by Tikhonov regularization. This set of distance distributions and the corresponding form factor fits is used to construct the total penalty function diagram (Fig. 1) for the calibration of DFOCs.

The essential steps of the calibration procedure are visualized in Fig. 1. The individual penalty functions are calculated to address the quality of the form factor fit (both in time and frequency domain, Fig. 1a, b) and the artifacts in the distance distribution (Fig. 1c, d). The four individual penalty functions are combined by multiplication to yield the total penalty function (Fig. 1e). The best set(s) of DFOCs corresponds to the minimum of this total penalty function. Note, the additional restriction of the space of DFOCs in the total penalty diagram is (Fig. 1e) due to the upper-distance penalty function, as explained below.

We should first discuss in detail the key data analysis steps in the RIDME experiment, and give some estimates in the underlying uncertainties.

3.2. Step 1: Background correction

The most common first step in the analysis of PDS data is the fitting of background, followed by the determination of the form factor trace, although joint fitting of the background and form factor has been proposed as well [34,35]. It is also possible to rather accurately estimate the intermolecular background contributions by measuring monoradical solutions of the same bulk spin concentration. [15,35] There are however two important remarks to this latter approach. First, frozen solutions of mono- and bi-radicals are not exactly identical samples. Second, it is well known in DEER spectroscopy that for time traces with several clear oscillations, as it is the case for our data, small errors in the background function do not affect the resulting distance distribution. In the case of RIDME, the analogous case would appear if we fit the distance distribution with a fixed set of DFOCs. However, for the calibration of the DFOCs, small variations of the intermolecular background can affect the final best DFOCs set. Therefore, fitting the intermolecular

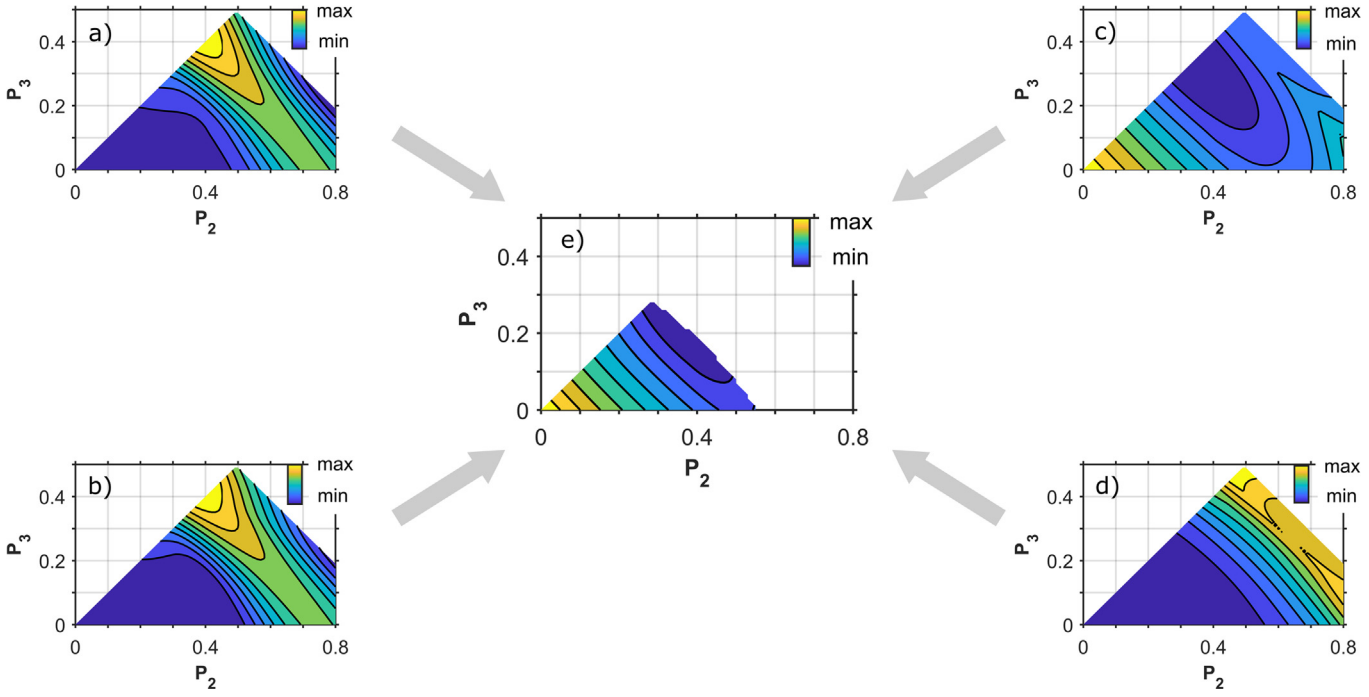

Fig. 1. A schematic workflow for calibrating DFOCs, illustrated for the Gd-PyMTA-based ruler with 4.3 nm interspin distance. (a) and (b) The r.m.s.d. plots for the form factor and the Pake pattern fit, respectively. (c) and (d) The lower-distance and upper-distance penalty functions, respectively. (e) The total penalty function. Contour lines correspond to 10% change with respect to the minimum of the r.m.s.d. value.

background to the actual RIDME traces of biradicals appears a safer approach.

The intermolecular background in the RIDME experiment can be described – to a good approximation – as a combination of two distributions, the first one formed by mono-exponential decay curves with different decay constants, and the second one formed by a distribution of different Gaussian decay curves [28]. In practice, RIDME background decay can be often fitted by a stretched exponential curve, provided the signal does not decay too close to zero. While RIDME background curves decaying down to approximately 20% of their initial intensity are sufficiently well fitted by one stretched exponential curve, the tail of the background decay trace demonstrates stronger deviations, so that fitting of the entire background trace required a sum of two stretched exponential functions [28]. Thus, for the best stability of the background fit, one should the time range in the experimental data where the RIDME signal decays to approx. 20% of its initial value and fitting by a single stretched exponential curve is feasible.

Depending on the selected background model, somewhat different form factor traces are obtained, which then result in somewhat different best sets of DFOCs. In order to determine the background model first, we performed a fitting of the resulting form factor traces that included only the contribution from the primary dipolar frequency, without any overtones (s. Experimental Details). This, of course, resulted in an unrealistic multi-peak distance distribution. Nonetheless, such a fit produced the best possible match to the experimental form factor trace that still conforms to the non-negativity restriction for the distance distribution. Examples of the background fits are given in the Supporting Information (Figs. S1-S7).

At this point, one should have obtained a set of background-corrected form factors, for which the form factor fitting with only primary frequency contributions produces r.m.s.d. values not exceeding the best one by more than a factor of two or so, as any of such fits would be approximately within the accuracy limits of the used model. However, we have omitted such a set of background-corrected form factors for two reasons. First, the uncertainty appearing at the step of actual calibration of DFOCs substantially exceeds the uncertainties due to different background correction (vide infra). Second, including such a set of different background models into the DFOCs fitting procedure would make the computational effort unrealistic. Thus, in the following procedure, we continue only with the form factors resulting from the background fit with lowest r.m.s.d. value (cf. Supporting Information).

3.3. Step 2: Quality of the form factor fit

In this next step, we take the background-corrected form factor trace and fit it with all possible combinations of the three DFOCs, i.e., P_1, P_2, and P_3. Note that up to eight DFOCs (if the zero-frequency contribution is counted in) can potentially contribute to the Gd(III)-Gd(III) RIDME form factor. However, the oscillatory part of the Gd(III)-Gd(III) RIDME signal stays nearly the same for different mixing times and temperatures, and contains only contributions from the three first non-zero frequency components. [27] Since we aim at analyzing the shape of the oscillatory part of the RIDME form factor and not the corresponding modulation depth, it is appropriate here to assume that the normalized oscillatory part of the form factor contains only the DFOCs one to three, with the sum of the three DFOCs equal to unity.

To assess the quality of the form factor fit, for each set of DFOCs, r.m.s.d. values were calculated. Both form factor fits, in the frequency and time domain, were considered in order to account for the very different distance dependence that the form factor function exhibit in the frequency and time domains. The r.m.s.d. plots (Fig. 1a and 1b) are constructed as a function of two DFOCs, which are independent due to the normalization $P_1 + P_2 + P_3 = 1$ (vide supra). The contour lines in Fig. 1a and 1b are drawn for the steps that correspond to a 10%-value of the lowest r.m.s.d. Obviously from Fig. 1a and 1b, multiple sets of DFOCs produce form factor fits that lie within this threshold of 10%, which is represented by a so-called "RIDME valley". This calculation demonstrates that, on the one hand, it is possible to roughly guess correct DFOCs for the given system by computing the form factor time-domain and frequency-domain 2D r.m.s.d. plots, but, on the other hand, this calculation is not enough to unambiguously determine the best DFOCs. In particular, we must know the shape of the underlying distance distribution for selecting the correct DFOCs within the RIDME valley.

3.4. Step 3: Intensities of the artifact distance peaks

Proper calibration of DFOCs requires the minimal deviation of the computed distance distribution from the anticipated one. Improper choice of DFOCs P_2 and P_3 leads to the artifacts in the distance distribution. If P_2 and P_3 are smaller than the true ones, the artifacts in the distance distribution are mainly placed at distances shorter than the true distance peak. As one or both of these DFOCs increase above its true values, stronger artifacts at the distances above the true distance peak appear [27]. However, also artifact peaks caused by other effects, such as background correction or insufficient ESEEM averaging, may be present. The position of such peaks would also be influenced by the DFOCs but for molecular rulers, as used in this work, the contribution of such additional artifacts is negligibly weak.

The best-solution set of DFOCs produces a distance distribution with the minimum probability to find a distance outside of the true distance peak. This criterion can be formalized in somewhat different ways, but, clearly, its usability relies on the fact that the true distance peak is narrow enough so that the artifact peaks are well resolved in the computed distance distribution. Here, we scaled all distance distributions, computed for different DFOC sets, for the same intensity of the true distance peak. Subsequently, each distribution was cut into two subdistributions at the expected distance. The upper- and lower-distance penalty functions (Fig. 1c, d) were calculated as the sum of distance probabilities of the subdistribution above and below the true distance maximum, respectively. Next, we identified all overestimated DFOC sets from the upper-distance penalty function by setting the threshold to 10% with respect to its minimum (Fig. 1d). Consequently, all DFOC sets that produce distance distributions with an upper-distance penalty function above the threshold are excluded, which was used to further restrict the space of DFOCs as shown in Fig. 1e.

3.5. Calibrated set of DFOCs

The best-solution set of DFOCs is then found from a total penalty function – a product of the four combined penalty functions pertaining to the form factor fits in time and frequency domain and the artifact distance peaks. The result is shown is Fig. 1e. Note, that the space of DFOCs is additionally restricted by excluding of the overestimated DFOCs, where the upper-distance penalty function was used. The requirement of the absence of artifact peaks helps to properly place the minimum of the total penalty function. Importantly, as has been already discussed qualitatively in the earlier report [27], a correlated change of P_2 and P_3 coefficients, which does not modify the sum $P_2 + P_3$, has only a very weak influence on the value of the penalty function. In other words, this calibration procedure can relatively well restrain the values for P_1 and the sum $P_2 + P_3$, but it leaves more uncertainty for the particular values of P_2 and P_3.

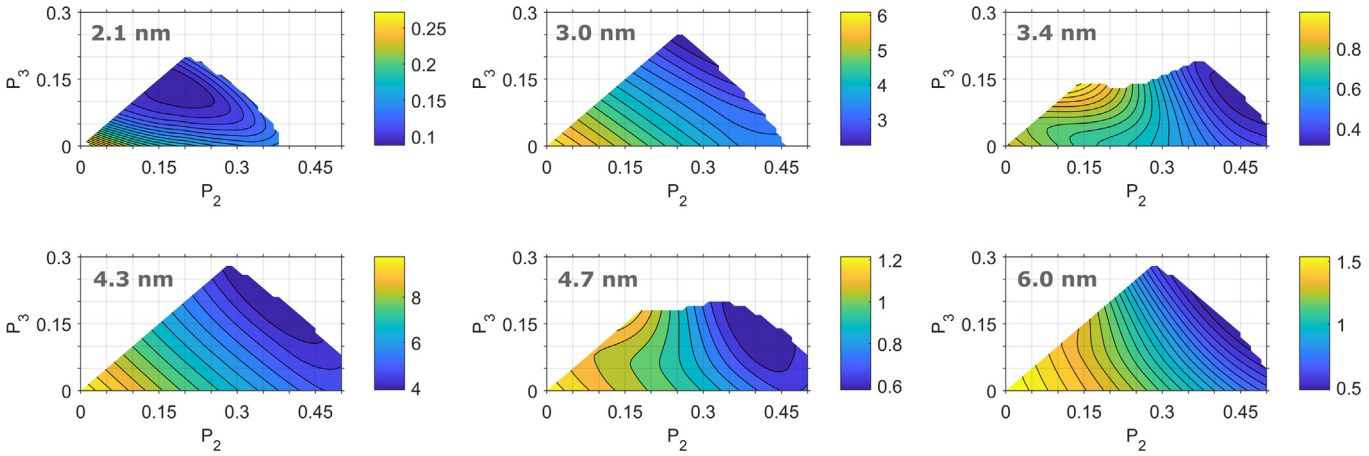

Fig. 2. Total-penalty functions for a series of Gd-PyMTA-based rulers in D_2O. The contour lines correspond to 10% change with respect to the minimum of the total-penalty function. The magnitude of the total-penalty function is color-coded.

3.6. Calibration of DFOCs for Gd(III)-PyMTA-based rulers

3.6.1. A series of molecular rulers

The above described systematic r.m.s.d.-based analysis was conducted for Gd-PyMTA-based rulers in the deuterated matrix D_2O, which cover the distance range from 2.1 to 6.0 nm. Fig. 2 shows 2D total-penalty function plots for these molecular rulers. In each case, the RIDME valley, as obtained by taking into account the quality of the fit and artifacts in the distance distribution, is clearly visible. The dark blue area corresponds to 10% deviation from the best r.m.s.d.-value and determines the pool of DFOCs that satisfy calibration conditions.

For molecular rulers with distances above 3 nm, the RIDME valley is situated at roughly the same place (Fig. 2) suggesting that the DFOCs for distances above 3 nm can be taken the same. This is in perfect agreement with earlier observations that DFOCs become distance-independent for distances above 3 nm [27]. The contour lines in the 2D total-penalty diagrams run approximately diagonally to P_2 and P_3 axes which points to the fact the penalty function is only weakly changing for the correlated change of P_2 and P_3 (and a constant P_1), especially at distances above 3 nm [27].

The best values for the DFOCs, which correspond to the minimum of the RIDME valley, are given in Table 2. Fig. 3 shows the best values for the P_1 coefficient together with error bars that were derived from the size of the RIDME valley (as described in the Experimental Section). The P_1 coefficient is constant for distances above 3 nm and becomes larger at shorter distances. This distance dependence can be partially explained by the limited excitation bandwidth of the microwave pulses used in the RIDME experiment. Consider Pake patterns for the basic dipolar frequency and the two overtones: The width of the Pake patterns becomes broader for shorter distances. At distance below 3 nm, the width of the Pake patterns belonging to the overtones exceeds the excitation bandwidth of the microwave pulses. Consequently, overtone frequencies get lost during the RIDME experiment and their contribution to the measured signal becomes lower. Because of the normalization condition $P_1 + P_2 + P_3 = 1$, the relative contribution of the basic dipolar frequency becomes larger and the P_1 coefficient grows (see Supporting Information). Note that for short spin-spin distances, the DFOCs are affected by both the limited excitation bandwidth and the previously mentioned balance of spin flips (vide supra).

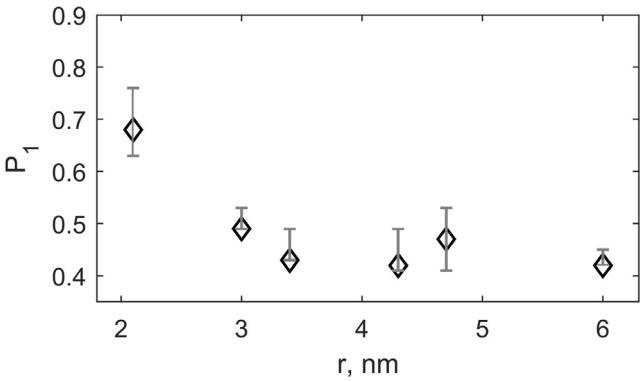

Fig. 3. The P_1 coefficient as a function of the interspin distance. Error bars indicate the range for P_1 within the 10% area (cf. Fig. 2).

The proposed r.m.s.d.-based calibration approach provides not only the best set of the DFOCs but is also an estimation of realistic uncertainties for the DFOCs. The RIDME valley contains all the DFOCs sets that fall within the uncertainty of the calibration procedure. Noteworthy, the DFOCs obtained from the r.m.s.d.-based calibration and manual calibration are found within the RIDME valley. The mean value of $P_1 = 0.44$ averaged over all distances above 3 nm (Table 2) is somewhat lower than previously proposed $P_1 = 0.51$ [27], but both values lie essentially within the error bar of the current calibration procedure. The difference between the two values comes from different calibration approaches: While the r.m.s.d.-based approach considers the form-factor fit in both domains, the manual approach considers the frequency domain (Pake pattern) focusing on the clearly resolved "horn-like" features.

Table 2
Overtone coefficients at the minimum of the RIDME valley as a function of the interspin distance for the deuterated samples.

Distance, nm	2.1	3.0	3.4	4.3	4.7	6.0
P_1	0.68	0.49	0.43	0.42	0.47	0.42
P_2	0.20	0.29	0.42	0.38	0.39	0.43
P_3	0.12	0.22	0.15	0.20	0.14	0.15

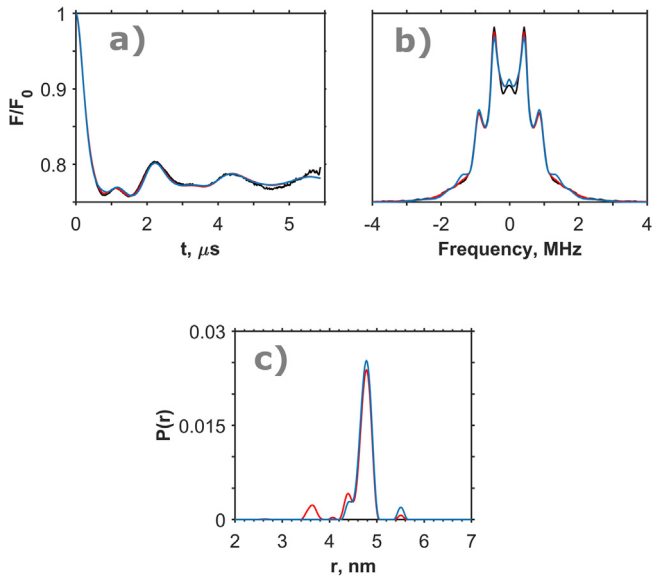

Fig. 4. Comparative processing of the RIDME data for the Gd-PyMTA-based ruler with the expected distance of 4.7 nm: (a) the form factor, (b) the Pake pattern, (c) the distance distribution. Black – experimental data, colored – processed data with DFOCs from the 10% area [0.51 0.40 0.09] [27] (red) and from the averaged minimum of the total-penalty diagrams [0.44 0.41 0.15] (blue).

Indeed, using either the earlier proposed DFOCs [0.51 0.40 0.09] or obtained here [0.44 0.41 0.15] provides almost identical distance distributions (Fig. 4). The form-factor fits in time and frequency domains reproduce experimental data very well. The fit of the Pake pattern with the previously reported set [0.51 0.40 0.09] (Fig. 4b, red) reproduces the "horn-like" features somewhat better, as expected for the manual approach. Overall, the slight differences in the fits result in the slight differences in the distance distributions. Here, only satellite peaks are affected, wereas the main peak at the expected distance is perfectly reproduced with both DFOCs sets.

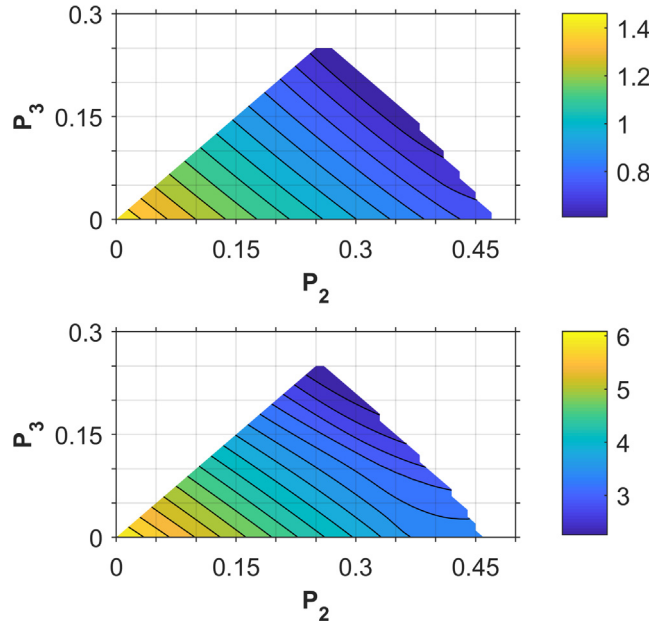

Fig. 5. Total-penalty diagrams for a Gd-ruler with the expected interspin distance of 3.0 nm measured in (top) H_2O and (bottom) D_2O.

3.6.2. Deuterated vs. protonated matrix

An example of the comparison of the DFOCs 2D total-penalty function plots for the cases of protonated and deuterated solvent are shown in Fig. 5. While the positions of the minima are not the same for these two plots, one can notice that realistic error bars of the DFOCs calibration exceed this difference. We can thus conclude that while it is not possible to state whether the DFOCs in these two samples are exactly the same, they are very similar, and for all practical purposes it is sufficient to use the same set of DFOCs for the cases of protonated and deuterated solvents.

Of course, here, the near identity of the DFOCs for protonated and deuterated samples is only shown for one type of Gd(III) complex. This should be, in principle, verified again, whenever a different type of Gd(III) complex is in use. Should this be a general rule for many such complexes, the DFOCs calibration procedure could be performed on the deuterated ruler solutions, and its results can be used also for the protonated solvent cases, e.g. in cells. Such a calibration procedure would require only about half the effort of calibrating the DFOCs separately for protonated and deuterated solutions.

4. Conclusions

We have presented a general r.m.s.d.-based procedure to calibrate the DFOCs and estimate the trust regions for RIDME experiments with Gd(III) complexes. From this procedure, the pool of DFOC sets – the RIDME valley in the total-penalty diagram – can be obtained that is suitable to extract interspin distances from the RIDME experiment. Importantly, the DFOCs in deuterated and protonated solvents can be assumed the same, which follows from the large cross-section of the respective RIDME valleys. For future experiments, we recommend to use the DFOC set [0.44 0.41 0.15] that corresponds to the averaged minimum of the RIDME valleys for distances above 3 nm. The results of the reported calibration procedure should be transferred with care to other Gd(III) complexes. The calibration procedure itself should perform the same for the spectroscopically similar Mn(II) complexes.

Declaration of Competing Interest

The authors declare that they have no known competing financial interests or personal relationships that could have appeared to influence the work reported in this paper.

Acknowledgement

The work was supported by the Swiss National Science Foundation (grant 200020169057) and by the Deutsche Forschungsgemeinschaft (DFG) within SPP 1601 (GO555/6-2). We are grateful to Prof. Dr. G. Jeschke for reading the manuscript and for helpful discussions.

Appendix A. Supplementary material

Supplementary data to this article can be found online at https://doi.org/10.1016/j.jmr.2022.107217.

References

[1] G. Jeschke, DEER distance measurements on proteins, in: M.A. Johnson, T.J. Martinez (Eds.), Annual Review of Physical Chemistry, vol. 63; Annual Reviews, Palo Alto, 2012, pp. 419–446.
[2] O. Schiemann, T.F. Prisner, Long-range distance determinations in biomacromolecules by EPR spectroscopy, Q Rev. Biophys. 40 (2007) 1–53.
[3] W.L. Hubbell, C.J. Lopez, C. Altenbach, Z.Y. Yang, Technological advances in site-directed spin labeling of proteins, Curr. Opin. Struct. Biol. 23 (2013) 725–733.

[4] P. Roser, M.J. Schmidt, M. Drescher, D. Summerer, Site-directed spin labeling of proteins for distance measurements in vitro and in cells, Org. Biomol. Chem. 14 (2016) 5468–5476.
[5] A.J. Fielding, M.G. Concilio, G. Heaven, M.A. Hollas, New Developments in Spin Labels for Pulsed Dipolar EPR, Molecules 19 (2014) 16998–17025.
[6] S. Bleicken, G. Jeschke, C. Stegmueller, R. Salvador-Gallego, A.J. Garcia-Saez, E. Bordignon, Structural model of active Bax at the membrane, Mol. Cell 56 (2014) 496–505.
[7] L.A. Lavery, J.R. Partridge, T.A. Ramelot, D. Elnatan, M.A. Kennedy, D.A. Agard, Structural asymmetry in the closed state of mitochondrial Hsp90 (TRAP1) supports a two-step ATP hydrolysis mechanism, Mol. Cell 53 (2014) 330–343.
[8] O. Duss, E. Michel, M. Yulikov, M. Schubert, G. Jeschke, F.H.T. Allain, Structural basis of the non-coding RNA RsmZ acting as a protein sponge, Nature 509 (2014) 588.
[9] K.L. Durr, L. Chen, R.A. Stein, R. De Zorzi, I.M. Folea, T. Walz, H.S. McHaourab, E. Gouaux, Structure and dynamics of AMPA receptor GluA2 in resting, Pre-open, and desensitized states, Cell 158 (2014) 778–792.
[10] M. Yulikov, Spectroscopically orthogonal spin labels and distance measurements in biomolecules, in: B.C. Gilbert, V. Chechik, D.M. Murphy (Eds.), *Electron Paramagnetic Resonance, vol. 24*, Electron Paramagnetic Resonance-Specialist Periodical Report, Royal Soc Chemistry, Cambridge, 2015, pp. 1–31.
[11] I. Ritsch, D. Klose, H. Hintz, A. Godt, G. Jeschke, M. Yulikov, Pulsed EPR methods to study biomolecular interactions, Chimia 73 (2019) 268–276.
[12] M. Teucher, M. Qi, N. Cati, H. Hintz, A. Godt, E. Bordignon, Orthogonally spin-labeled rulers help to identify crosstalk signals and improve DEER signal fidelity, Magn. Reson. Discuss. (2020).
[13] D. Akhmetzyanov, H.Y.V. Ching, V. Denysenkov, P. Demay-Drouhard, H.C. Bertrand, L.C. Tabares, C. Policar, T.F. Prisner, S. Un, RIDME spectroscopy on high-spin Mn2+ centers, Phys. Chem. Chem. Phys. 18 (2016) 30857–30866.
[14] T. Wiegand, D. Lacabanne, K. Keller, R. Cadalbert, L. Lecoq, M. Yulikov, L. Terradot, G. Jeschke, B.H. Meier, A. Bockmann, Solid-state NMR and EPR Spectroscopy of Mn2+-Substituted ATP-Fueled Protein Engines, Angew. Chem. Int. Edit. 56 (2017) 3369–3373.
[15] A.V. Astashkin, Mapping the Structure of Metalloproteins with RIDME, in: P.Z. Qin, K. Warncke (Eds.), Methods in Enzymology, Elsevier Academic Press Inc, San Diego, vol. 563, 2015, pp. 251–284.
[16] D. Abdullin, P. Brehm, N. Fleck, S. Spicher, S. Grimme, O. Schiemann, Pulsed EPR dipolar spectroscopy on spin pairs with one highly anisotropic spin center: The low-spin Fe-III case, Chem.-Eur. J. 25 (2019) 14388–14398.
[17] D. Abdullin, H. Matsuoka, M. Yulikov, N. Fleck, C. Klein, S. Spicher, G. Hagelueken, S. Grimme, A. Lutzen, O. Schiemann, Pulsed EPR dipolar spectroscopy under the breakdown of the high-field approximation: The high-spin iron(III) case, Chem.-Eur. J. 25 (2019) 8820–8828.
[18] T.F. Cunningham, M.R. Putterman, A. Desai, W.S. Horne, S. Saxena, The double-histidine Cu2+-binding motif: A highly rigid, site-specific spin probe for electron spin resonance distance measurements, Angew. Chem. Int. Edit. 54 (2015) 6330–6334.
[19] L. Garbuio, K. Zimmermann, D. Haussinger, M. Yulikov, Gd(III) complexes for electron-electron dipolar spectroscopy: Effects of deuteration, pH and zero field splitting, J. Magn. Reson. 259 (2015) 163–173.
[20] A. Feintuch, G. Otting, D. Goldfarb, Gd3+ Spin Labeling for Measuring Distances in Biomacromolecules: Why and How?, Method Enzymol 563 (2015) 415–457.
[21] W.P. Cacheris, S.C. Quay, S.M. Rocklage, The relationship between thermodynamics and the toxicity of gadolinium complexes, Magn. Reson. Imaging 8 (1990) 467–481.
[22] J.C. Bousquet, S. Saini, D.D. Stark, P.F. Hahn, M. Nigam, J. Wittenberg, J.T. Ferrucci, GD-DOTA - Characterization of a new paramagnetic complex, Radiology 166 (1988) 693–698.
[23] H.J. Weinmann, R.C. Brasch, W.R. Press, G.E. Wesbey, Charateristics of gadolinium-DTPA complex - A potential NMR contrast agent, Am. J. Roentgenol. 142 (1984) 619–624.
[24] L.V. Kulik, S.A. Dzuba, I.A. Grigoryev, Y.D. Tsvetkov, Electron dipole-dipole interaction in ESEEM of nitroxide biradicals, Chem. Phys. Lett. 343 (2001) 315–324.
[25] S. Milikisyants, F. Scarpelli, M.G. Finiguerra, M. Ubbink, M. Huber, A pulsed EPR method to determine distances between paramagnetic centers with strong spectral anisotropy and radicals: The dead-time free RIDME sequence, J. Magn. Reson. 201 (2009) 48–56.
[26] S. Razzaghi, M. Qi, A.I. Nalepa, A. Godt, G. Jeschke, A. Savitsky, M. Yulikov, RIDME spectroscopy with Gd(III) centers, J. Phys. Chem. Lett. 5 (2014) 3970–3975.
[27] K. Keller, V. Mertens, M. Qi, A.I. Nalepa, A. Godt, A. Savitsky, G. Jeschke, M. Yulikov, Computing distance distributions from dipolar evolution data with overtones: RIDME spectroscopy with Gd(III)-based spin labels, Phys. Chem. Chem. Phys. 19 (2017) 17856–17876.
[28] K. Keller, M. Qi, C. Gmeiner, I. Ritsch, A. Godt, G. Jeschke, A. Savitsky, M. Yulikov, Intermolecular background decay in RIDME experiments, Phys. Chem. Chem. Phys. 21 (2019) 8228–8245.
[29] A. Collauto, V. Frydman, M.D. Lee, E.H. Abdelkader, A. Feintuch, J.D. Swarbrick, B. Graham, G. Otting, D. Goldfarb, RIDME distance measurements using Gd(III) tags with a narrow central transition, Phys. Chem. Chem. Phys. 18 (2016) 19037–19049.
[30] M. Azarkh, A. Bieber, M. Qi, J.W.A. Fischer, M. Yulikov, A. Godt, M. Drescher, Gd (III)-Gd(III) Relaxation-Induced Dipolar Modulation Enhancement for In-Cell Electron Paramagnetic Resonance Distance Determination, J. Phys. Chem. Lett. 10 (2019) 1477–1481.
[31] A. Dalaloyan, M. Qi, S. Ruthstein, S. Vega, A. Godt, A. Feintuch, D. Goldfarb, Gd (III)-Gd(III) EPR distance measurements - the range of accessible distances and the impact of zero field splitting, Phys. Chem. Chem. Phys. 17 (2015) 18464–18476.
[32] M. Qi, M. Hülsmann, A. Godt, Spacers for geometrically well-defined water-soluble molecular rulers and their application, J. Org. Chem. 81 (2016) 2549–2571.
[33] M. Qi, M. Hülsmann, A. Godt, Synthesis and hydrolysis of 4-chloro-PyMTA and 4-iodo-PyMTA esters and their oxidative degradation with Cu(I/II) and oxygen, Synthesis 48 (2016) 3773–3784.
[34] L.F. Ibanez, G. Jeschke, Optimal background treatment in dipolar spectroscopy, Phys. Chem. Chem. Phys. 22 (2020) 1855–1868.
[35] G. Jeschke, V. Chechik, P. Ionita, A. Godt, H. Zimmermann, J. Banham, C.R. Timmel, D. Hilger, H. Jung, DeerAnalysis2006 - a comprehensive software package for analyzing pulsed ELDOR data, Appl. Magn. Reson. 30 (2006) 473–498.